

# Development of Doppler Wind Lidar Simulator for future space application

Shoken Ishii<sup>(a)</sup>, Sara Yamanaka<sup>(a)</sup>, Nami Tanoue<sup>(a)</sup>, Hideki Takenaka<sup>(a)</sup>, Koza Okamoto<sup>(b)</sup>,  
Izumi Okabe<sup>(b)</sup>, Atsushi Sato<sup>(c)</sup>, Tomoaki Nishizawa<sup>(d)</sup>, Yoshitaka Jin<sup>(d)</sup>, and Hajime Okamoto<sup>(e)</sup>

<sup>(a)</sup> Tokyo Metropolitan University

6-6 Asahigaoka, Hino-shi, Tokyo, 191-0065, Japan

<sup>(b)</sup> Meteorological Research Institute of Japan Meteorological Agency

1-1 Nagamine, Tsukuba, Ibaraki 305-0052, Japan

<sup>(c)</sup> Tohoku Institute of Technology

5-1, Yagiyama Kasumi-cho, Taihaku-ku, Sendai, Miyagi, 982-8577, Japan

<sup>(d)</sup> National Institute for Environmental Studies

16-2 Ogawa, Tsukuba, Ibaraki, 305-8506, Japan

<sup>(e)</sup> Kyushu University

6-1 Kasuga-koen Kasuga, Fukuoka, 816-8580, Japan

sishii@tmu.ac.jp

**Abstract:** Wind is one of fundamental meteorological elements describing the atmospheric state. Global wind observation is important to improve the initial conditions essential for numerical weather prediction (NWP), climate studies, and meteorological studies. A space-based Doppler Wind Lidar (DWL) would be a useful approach for global wind profiling. It is important to evaluate wind measurement performance before launch of space-based DWL. We develop coherent and direct-detection DWL simulators to investigate measurement performance on wind. In the paper, we describe the development of the two DWL simulators for the future space application.

## 1. Introduction

An integrated global 3D observing system including wind observations with higher spatial resolution is required for understanding detailed atmospheric conditions. In last decades, the role of satellite observing systems has been increased, and they heavily contribute to the reduction of prediction errors.

The World Meteorological Organization (WMO) Integrated Global Observing System (WIGOS) plan summarized by the WMO states that it is important to promote continuous and effective satellite observing systems, and to improve observation performance. Satellite wind observing systems use tracking clouds or water vapor (Atmospheric Motion Vectors, AMVs), which can observe over a wide area and at high frequency. However, it has problems such as height assignment, vertical resolution, system accuracy, and wind measurement over clear/dry regions and at specific limited layers.

It is expected that a hyper-infrared sounder planned to be installed on the next geostationary meteorological satellite Himawari will improve these issues of AMVs,

but the height assignment error in AMVs remains as critical issue.

The European Space Agency (ESA) launched the Aeolus mounted a space-based Doppler wind lidar (DWL) [1-2] in August 2018 with the objective of improving the initial global wind input for the NWP and deepening the understanding and modeling of atmospheric dynamics phenomena at global and regional scales. The Aeolus has realized the global wind profiling from space and has demonstrated importance of the global wind profiling and great effects of the DWL in improving the accuracy of NWP and the application to atmospheric dynamics. The Aeolus has been operated over its three-year design life, and it ended its mission life in July 2023. ESA is considering a next-generation DWL mission. The Japan Aerospace Exploration Agency (JAXA) has conducted feasibility study of a space-based coherent DWL (hereafter CDWL) that uses a detection method different from Aeolus [3-5]. In the paper, the development of the two DWL simulators is described to evaluate measurement performance on wind.

## 2. Doppler wind lidar

A DWL is a useful remote sensing technique for measuring line-of-sight (LOS) wind speed, and it provides wind profiles with good vertical and temporal resolutions. When a laser beam transmitted from a DWL is applied to atmospheric wind-carried atmospheric molecules, aerosols, and clouds, backscattered light shifts slightly from the original frequency of the transmitted laser at the time of emission, due to the Doppler effect. Atmospheric molecular (Rayleigh-Brillouin scattering, hereafter RBS scattering) and aerosol and cloud (Mie scattering) backscatter spectra are shown in Figure 1. The Doppler frequency shift  $f_D$  directly determines the LOS component  $v_{LOS}$  of the wind vector. The Doppler frequency shift  $f_D$  is given by

$$f_D = 2 \cdot f_L \frac{v_{LOS}}{c} = 2 \cdot \frac{v_{LOS}}{\lambda_L} \quad (1)$$

where  $f_L$  and  $\lambda_L$  are the frequency and wavelength of the transmitted laser, and  $c$  is the speed of the light. At a laser wavelength  $\lambda_L$  of 354.8 nm ( $f_L=844.862$  THz) and 2051.3 nm ( $f_L=146.155$  THz), a LOS wind speed of 1 m/s corresponded to a Doppler-shifted frequency of 5.636 and 0.975 MHz, respectively.

There are two types of DWL according to detection techniques: heterodyne-detection for CDWL and direct-detection for direct-detection DWL (DDWL). The CDWL with an optical heterodyne technique uses Mie scattering to measure LOS wind speed. The CDWL measures the LOS wind speed with components of the background atmospheric flow. The measurement accuracy of the CDWL depends on the load of aerosols and clouds. The CDWL is suitable for wind measurements in the low and middle troposphere.

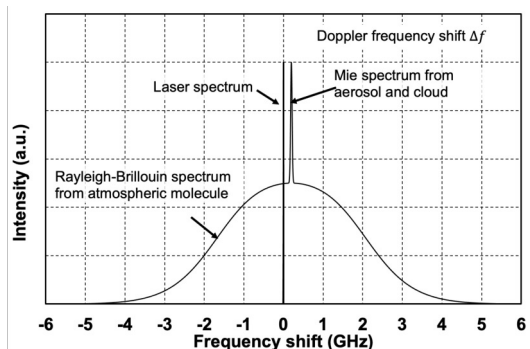


Figure 1. Principle of DWL wind measurement using the Rayleigh-Brillouin spectrum from

atmospheric molecule, Mie spectrum from aerosol and cloud, and laser spectrum.

The DDWL uses both RBS and Mie scattering to make wind measurements. The DDWL based on the RBS scattering has advantages for wind measurement in the middle and upper troposphere and the lower stratosphere, which provides us a LOS wind speed of background atmospheric flow. There are several types of spectral filters used in receiver techniques, such as Fabry-Perot etalon interferometer, Fizeau interferometer Mach-Zehnder interferometer, and so on. The DDWL with a double-edge receiver uses a frequency discriminator based on the double-edge Fabry-Pérot etalon technique in the paper.

## 3. Coherent Doppler wind lidar simulator

We developed a end-to-end comprehensive CDWL simulator to resolve the issues and to evaluate wind measurement performance from space. The coherent signal is well approximated as a zero-mean complex Gaussian random vector  $z$  with elements, complex coherent signal,  $z_k$  satisfying  $\langle z_k z_k^* \rangle = 0$ . We assume that the coherent signal is stationary. We use complex coherent signal in the CDWL-Sim. The coherent signal is expressed as the following discrete time series,

$$z_k = s_k \exp(i2\pi f_D \cdot kT_s) + n_k \quad , \quad (2)$$

where  $T_s$  is the sampling interval, and random signal  $s_k$  is independent of the uncorrelated noise  $n_k$  with Gaussian white noise ( $|z_k z_k^*| = 1$ ). The average noise power is set to unity to simplify the results.

The covariance  $R_{i,k}$  of the coherent signal at a range gate  $l$  reduces to

$$R_{l,k} = SNR_{C,l} \rho_k \exp(i2\pi f_D kT_s) + N_k \quad , \quad (3)$$

where  $SNR_{C,l}$  is the signal-to-noise ratio,  $\rho_k$  is the normalized covariance of the coherent signal. The  $R_{l,k}$  is converted to the power spectra of the coherent signal using the FFT. The power spectra  $Y_m$  with  $m$  as index is given as follows,

$$Y_m = \frac{1}{2M} \sum_{k=0}^{2M-1} R_{l,k} \exp\left(-i2\pi \frac{m}{2M} k\right) \quad . \quad (4)$$

The power spectra of the coherent signal is converted to the time-domain using the inverse

FFT. The time-domain coherent signal  $z_{l,k}$  is given as the follows,

$$z_{l,k} = \sum_{m=0}^{2M-1} y_m \exp\left(i2\pi \frac{m}{2M} k\right) \quad , \quad (5)$$

where  $M$  is the sampling number at the range gate  $l$ . The power spectra density  $PSD_{l,k}$  is calculated given by Eq. (6),

$$PSD_{l,k} = \frac{T_s}{2M} \left| \sum_{k=0}^{2M-1} z_{l,k} \exp\left(-i2\pi \frac{m}{2M} k\right) \right|^2 \quad , \quad (6)$$

and is averaged according to the spatiotemporal resolution meeting the WMO user requirements. Finally, average Doppler frequency shift and width of the  $PSD_{l,k}$  is determined using the maximum likelihood estimation method. The width is defined as a wind speed error in the simulation.

#### 4. Direct-detection Doppler wind lidar simulator

The Aeolus carries the Atmospheric Laser Doppler Instrument (ALADIN), which uses a single-frequency ultraviolet (UV) laser and a direct-detection system with two interferometers, namely, a FPEI for the RBS scattering signals (Rayleigh-channel) and a Fizeau interferometer for the Mie scattering signals (Mie-channel). The double-edge and fringe-imaging techniques are used for the Rayleigh- and Mie-channels. The Rayleigh-channel can provide us LOS wind speed profiles from the ground up to an altitude of approximately 30 km under the clear-sky condition. The Aeolus ended its mission life in July 2023. ESA is considering a next-generation space-based DWL as an Aeolus follow-on mission.

We are developing an end-to-end DDWL simulator with the National Institute for Environmental Studies (NISE) and the Kyushu University (KU) to design systematic specifications a DDWL and to evaluate wind measurement performance for future synergetic wind observation between the space-based CDWL, and the Aeolus follow-on and the next-generation Himawari.

The double-edge technique with Fabry-Perot etalon interferometer is used in the DDWL simulator. The Michelson interferometer is also used to reduce the contamination from the Mie scattering signal. The spectrum from Mie

scattering is assumed to be narrow in comparison with the laser line spectrum, the convolution operation between the two spectra is neglected in the following discussions. The number of photoelectrons  $N_{i=1,2}(r)$  detected at the two detectors for a LOS wind speed  $v_{LOS}(r)$  is given as

$$N_i(r, f_D) = K_i \frac{E_T}{hf_L} \cdot \frac{A_R}{r^2} \cdot \Delta r \cdot T_{Atmos}^2 \cdot \int_{-\infty}^{\infty} \{\beta_{RBS}(r) \cdot T_i(f) \cdot G_L * G_{RBS}(r, f, f_D) + \beta_{Mie}(r) \cdot T_i(f) \cdot G_L * L_{Mie}(r, f, f_D)\} df \quad , \quad (7)$$

where  $K_i$  is a system constant for channel 1 and 2,  $E_T$  is the laser output energy,  $A_R$  is the telescope area,  $\Delta r$  is the one range gate,  $r$  is the distance to the target atmosphere,  $T_{Atmos}$  is the atmospheric transmission, and  $T_i(f)$  is the transmission at the frequency of  $f$  for optical filter centered at  $f_L$ .  $\beta_{RBS}$  and  $\beta_{Mie}$  are the RBS and Mie backscattering coefficients,  $G_L$  and  $G_{RBS}$  are Gaussian line-broadening functions for the laser spectral width and the RBS spectrum,  $L_{Mie}$  is a Lorentzian function for the Mie spectrum, the asterisk denotes a convolution operation, and  $h$  is Planck's constant.

The LOS wind speed error  $\sigma_{LOS}(r, f_D)$  (m/s) is given by Eq. (8),

$$\sigma_{LOS}(r, f_D) = \frac{1}{\frac{5.639 \times 10^6 \text{ Hz}}{1 \frac{\text{m}}{\text{s}}} \cdot (\vartheta_1 + \vartheta_2)} \cdot \sqrt{\frac{1}{SNR_{D,1}(r)^2} + \frac{1}{SNR_{D,2}(r)^2}} \quad , \quad (8)$$

where  $SNR_{D,i=1,2}(r)$  is the signal-to-noise ratio (SNR) for each channel. In the study, we assume that shot noise was the dominant noise source. The random errors of  $N_i(r, f, \Delta f)$  were described by a Poisson distribution. The SNR is given by Eq. (9)

$$SNR_{D,i}(r) = \frac{N_i(r, v, \Delta v)}{\sqrt{N_i(r, v, \Delta v)}} = \sqrt{N_i(r, v, \Delta v)} \quad . \quad (9)$$

#### 5. Result

We conducted preliminary simulations to confirm their operation and to investigate wind measurement performance using the CDWL and DDWL simulators. The conceptual parameters of the space-based CDWL and DDWL are listed summarized in Table 1. Figure 2(a) shows the target wind profile model. The strong wind blows around at an altitude of

10 km [6]. Figures 2(b) and 2 (c) show results of wind measurement performance simulated using the parameters listed in Table 1, enhanced aerosol model [6], and US standard atmosphere 1976 [7]. Black and blue bars show wind speed errors. The results show that both the CDWL and DDWL simulators can retrieve the target wind profile model successfully. We found that those simulators execute proper simulations. The CDWL simulator shows wind speed errors of 0.7 m/s in the BL and 1 to 2 m/s in the FT,

**Table 1. Summary of space-based coherent and direct-detection DDWLs**

Wavelength ( $\mu\text{m}$ )	2	0.355
Pulse energy (J)	90	80
PRF (Hz)	30 x 2	50.5
Telescope diameter (m)	0.6	1.5
Total system efficiency	0.04	0.05
Satellite orbit (km)	300	400
Azimuth angle ( $^\circ$ )		90
Nadir angle ( $^\circ$ )		35
Horizontal resolution (km)		<100
Vertical resolution (km)	BL: <0.5 FT: <1	FT, LST: 1

BL: Boundary layer, FT: Free troposphere, LST: Lower stratosphere

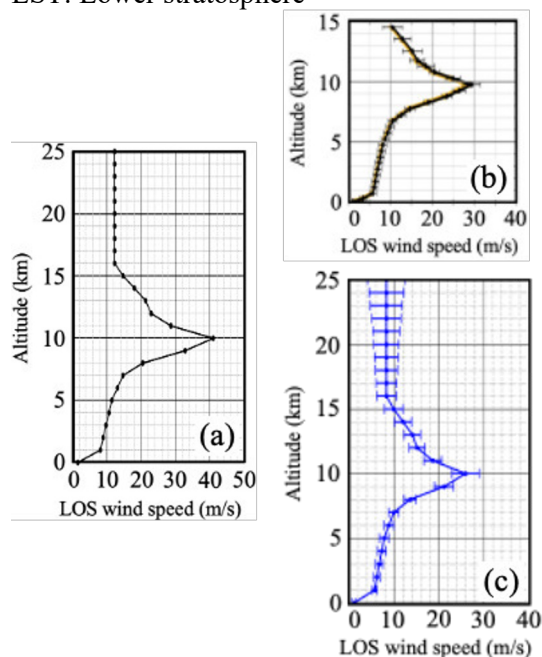


Figure 2. Wind profiles estimated using (a) target wind profile, (b) CDWL, and (c) DDWL simulators with the double-edge technique.

while the DDWL simulator shows wind speed errors of 1 m/s in the BL and 1 to 3 m/s in the FT and LST except for altitudes of 9 and 10 km.

## 6. Summary

JMA will launch the geostationary meteorological satellite Himawari in the late 2020. ESA is considering a Aeolus follo-on mission in the early 2030. In Japan, the working group continues to make feasibility study to launch the space-based coherent DWL in the 2030s. We develop coherent and direct-detection DWL simulators to investigate wind measurement performance for the future wind observation from space to discuss synergy wind measurement each other. We conducted preliminary 1-D simulations to investigate wind measurement performance using the two simulators. The results are wind speed errors of 0.7 m/s in the BL and 1 to 2 m/s in the FT for the CDWL and 1 m/s in the BL and 1 to 3 m/s in the FT and LST for the DDW. We develop to conduct 3-D simulations using the two simulators to enhance the feasibility of the space-based CDWL.

## 7. References

- [1] ESA, Atmospheric dynamics mission. Mission Selection Rep. ESA SP-I233(4), (1999).
- [2] A. Stoffelen, J. Pailleux, E. Kallen, M. J. Vaughan, L. Isaksen, P. Flamant, W. Wergen, E. Andersson, H. Schyberg, A. Culoma, R. Meynard, M. Endemann, and P. Ingmann, "The atmospheric dynamics mission for global wind field measurement," *BAMS*, **86**, 73-87 (2005).
- [3] S. Ishii, P. Baron, M. Aoki, K. Mizutani, M. Yasui, S. Ochiai, A. Sato, Y. Satoh, T. Kubota, D. Sakaizawa, R. Oki, K. Okamoto, T. Ishibashi, T. Y. Tanaka, T. T. Sekiyama, T. Maki, K. Yamashita, T. Nishizawa, M. Satoh, and T. Iwasaki, "Feasibility study for future space-borne coherent Doppler wind lidar, part 1: instrumental overview for global wind profile observation," *JMSJ*, **95**, 301-317 (2017).
- [4] P. Baron, S. Ishii, K. Okamoto, K. Gamo, K. Mizutani, C. Takahashi, T. Itabe, T. Iwasaki, T. Maki, R. Oki, S. Ochiai, D. Sakaizawa, M. Satoh, Y. Satoh, T. Tanaka, and M. Yasui, "Feasibility study for future spaceborne coherent Doppler wind lidar, part 2: measurement simulation algorithms and retrieval error characterization," *JMSJ*, **95**, 319-342 (2017).
- [5] K. Okamoto, T. Ishibashi, S. Ishii, P. Baron, K. Gamo, T. Y. Tanaka, Y. Yamashita, and T. Kubota, "Feasibility study for future space-borne coherent Doppler wind lidar, part 3: impact assessment using sensitivity observing system simulation experiments," *JMSJ*, **96**, 179-199 (2018).
- [6] G. D. Emmitt, J. Spinhirne, R. Menzies, D. Winker, and D. Bowdle, "Target atmospheres for use in Doppler wind lidar (DWL) concept studies," [www.swa.com/images/LidarSpaceBased/TARGET\\_ATMOSPHERES\\_DWL\\_CONCEPT\\_STUDIES.pdf](http://www.swa.com/images/LidarSpaceBased/TARGET_ATMOSPHERES_DWL_CONCEPT_STUDIES.pdf), accessed on March 4 2024.
- [7] U.S. Standard Atmosphere, 1976, U.S. Government Printing Office, Washington, D. C., 1976.